International Journal of Plasticity 29 (2012) 102–119

Contents lists available at SciVerse ScienceDirect

International Journal of Plasticity

journal homepage: www.elsevier.com/locate/ijplas

Computational homogenization of elasto-plastic porous metals

Felix Fritzen [a,*], Samuel Forest [b], Thomas Böhlke [a], Djimedo Kondo [c], Toufik Kanit [d]

[a] Chair for Continuum Mechanics, Institute of Engineering Mechanics, Karlsruhe Institute of Technology (KIT), Germany
[b] Mines ParisTech CNRS, Centre des Matériaux UMR 7633, BP87 91003 Evry, France
[c] Institut d'Alembert, UMR 7190 CNRS, UPMC, Tour 55/65, 4, Place Jussieu, Boîte 162, 75252 Paris Cedex 05, France
[d] Laboratoire de Mécanique de Lille, UMR 8107 CNRS, USTL, 59650 Villeneuve d'Ascq, France

ARTICLE INFO

Article history:
Received 18 January 2011
Received in final revised form 15 August 2011
Available online 31 August 2011

Keywords:
Ductile porous metals
Computational homogenization
Plasticity
Finite element method
Representativeness

ABSTRACT

The effective material response of ductile metals containing spherical pores at volume fractions between 0.1% and 30% is investigated on a computational basis. Periodic hard core models of spherical voids are used in a Monte Carlo type finite element study. The objective of the study is the investigation of the pressure dependency of the deviatoric limit stress of the three-dimensional microstructures. In order to characterize the underlying morphology, the statistical properties of the unit cells are evaluated. The representativeness of the computational results is investigated. With respect to the local material response, the inelastic deformations within the unit cell are analyzed and compared for different types of boundary conditions. The computational results are related to existing analytical models and an extension of the Gurson–Tvergaard–Needleman model is proposed to overcome the observed discrepancies. The new model has only one additional parameter, and is found to efficiently predict the pressure dependency of the limit stress for all examined porosities.

1. Introduction

The mechanical properties of ductile porous engineering materials have been extensively studied in the last decades. The aim of these studies is the prediction of the inelastic deformation of macroscopically homogeneous materials, while still accounting for a possibly evolving porosity on the small scale. An outcome of these models is the pressure dependence of the macroscopic yield stress of the porous material. In the pioneering work of Gurson (1977), a macroscopic criterion has been formulated for ductile porous media by using micro–macro Limit Analysis theory (LA). The Gurson derivation is based on an isotropic and plastically incompressible material obeying to a von Mises type plasticity law. The geometry of the considered model problems is given by a hollow sphere or cylinder subjected to a uniform macroscopic strain rate at its external boundary. The LA computation has been performed via a kinematic approach using simple radial trial velocity fields. As pointed out by Perrin (1992), the procedure leads to an upper bound of the macroscopic yield criterion of the porous material if a Hashin assemblage of composite spheres is considered. Later, a heuristic parametric modification of Gurson's criterion has been proposed by Tvergaard (1981) and Needleman and Tvergaard (1987) and led to the widely used Gurson–Tvergaard–Needleman (GTN) model. The identification of the parameters of the GTN model was frequently based on two-dimensional finite element simulations (e.g., Needleman and Tvergaard, 1984, 1987).

Recent review papers on ductile fracture models illustrate the wide variety of extensions of Gurson's model on the basis of enhanced homogenization schemes or of phenomenological pragmatic generalizations in order to incorporate, for example, viscoplasticity, kinematic hardening or anisotropic matrix behavior (e.g., Pardoen and Pineau, 2007; Monchiet et al., 2008, 2011; Besson, 2009, 2010; Benzerga and Leblond, 2010). Nonlinear homogenization approaches based on variational

* Corresponding author.
E-mail addresses: fritzen@itm.uni-kalrsruhe.de (F. Fritzen), boehlke@itm.uni-kalrsruhe.de (T. Böhlke).

0749-6419/$ - see front matter © 2011 Elsevier Ltd. All rights reserved.
doi:10.1016/j.ijplas.2011.08.005

techniques introduced by Ponte-Castañeda (1991) have been proposed for ductile porous media (see, e.g., Suquet, 1992). These variational techniques can be used to derive bounds on the actual material behavior. For example, Leblond et al. (1994) showed that Gurson's prediction may violate the bounds of Ponte-Castañeda (1991) for purely deviatoric loading. In order to overcome this deficiency a modification of the Gurson criterion has first been proposed by Leblond et al. (1994). Other upper bounds have been proposed by Michel and Suquet (1992) and Garajeu and Suquet (1997). More recently, the variational approach has been extended by Danas and Ponte-Castañeda (2009a,b) involving second order methods to provide estimates for the effective material response in a large deformation setting and while accounting for evolving pore shapes. Unfortunately, this method does not deliver closed-form expressions of the yield function and is, hence, not considered here. A major advantage of the theoretical approaches is their ability to provide rigorous lower and upper bounds of the macroscopic dissipation. In particular, the lower bound provided by Sun and Wang (1995) for the plasticity of porous metals is particularly well-suited for the discussion of the results found in the present work. However, the underlying microstructures are limited to the use of the same hollow sphere cell as for LA. Hence, they are not able to directly take into account interaction between voids.

In contrast to the large variety of theoretical developments in the field of ductile porous materials, it seems that rather little attention has been paid to the use of three-dimensional numerical methods to obtain a macroscopic yield function. Two-dimensional plane stress or plane strain models and axi-symmetric unit cells of single pores have frequently been used to identify numerical parameters or to verify theoretical results. More specifically, most of existing works are devoted to the hollow sphere cell (see for instance Gologanu et al., 1997; Guo et al., 2008) for macroscopically isotropic materials. Trillat and Pastor (2005) have conducted various numerical studies of plastic porous materials using both static and kinematic methods of LA for the hollow sphere. The objective of these authors was the numerical validation of upper and lower bounds of the macroscopic yield surface using kinematic and static boundary conditions. In particular, in Trillat and Pastor (2005), the Gurson criterion is shown to be relevant for materials whose microstructure can be represented by the hollow sphere model. Other works concerned with the influence of the third invariant of the macroscopic stress tensor have very recently been promoted by, e.g., Hsu et al. (2009) and Gao et al. (2009, 2011). Again no numerical studies on unit cell level involving multiple pores were performed. The numerical data used to examine the proposed models is based on numerical evidence of single pore models using different types of traction or displacement boundary conditions. Similarly, Seifert and Schmidt (2009) investigated the constitutive response of a single pore model under cyclic loading using a cuboidal unit cell. To our knowledge, notable applications of three-dimensional multi-pore models have only been published by Bilger et al. (2005, 2007) where the influence of pore clustering onto the macroscopic material response has been investigated. The respective periodic full field problems were solved using the Fast Fourier Transformation (FFT) massively used, e.g. by Moulinec and Suquet (1998) and modified for materials with infinite phase contrast by Michel et al. (2001).

More generally, computational homogenization methods rely on the testing of finite size volume elements containing a detailed distribution of material inhomogeneities. The question of the representativeness of such volumes arises in order to decide whether the found apparent material properties can be regarded as the wanted effective ones or not. In the used framework, the size of the representative volume element (RVE) is given by the number of heterogeneities. The minimum size of the RVE is of great interest and it depends on the complexity of phase distribution, on the investigated type of physical properties and on the targeted precision of the estimation of effective properties. Notably the geometry of the RVE has to be representative. This requirement can be considered as a necessary but not sufficient condition. In order to be macroscopically representative, the actual effective constitutive properties have to be considered. In the case of linear elasticity, the statistical approach initiated by Gusev (1997), Ren and Zheng (2002) and Kanit et al. (2003) is now well-established. It amounts to considering ensemble averages of the apparent properties of material volume elements with increasing size and investigating their convergence with respect to volume size. Boundary conditions play a central role in this procedure and it turns out that periodic boundary conditions generally provide faster convergence of ensemble averages if a sufficient number of realizations are considered for each volume size (Sab and Nedjar, 2005). Apparent properties based on homogeneous stress or strain boundary conditions are also informative because they can provide bounds for effective properties of specific types of materials (e.g. thermo-elastic or rigid-viscoplastic materials) as shown in (Hazanov and Huet, 1994; Kanit et al., 2006).

Estimations of RVE size, e.g. in terms of the number of heterogeneities that should be considered, for nonlinear mechanical properties in heterogeneous materials are seldom in the literature (Cailletaud et al., 2003). Two-phase highly contrasted nonlinear viscous materials were considered in (Madi et al., 2005; Jessell et al., 2009) and show that RVE sizes for nonlinear properties differ from sizes obtained in linear elasticity but can still be determined following the same statistical approach. For hardening elastic–plastic polycrystals, reliable tensile curves can be obtained from computations involving a few hundreds of grains (Cailletaud et al., 2003; Fritzen et al., 2009). However various loading conditions (tension, shear, multi-axial overall loading) should be considered in a systematic way, which has not been the case yet.

The question of RVE size for nonlinear composites displaying perfect plasticity behavior or even softening (damaging) behavior, and thus prone to strain localization, remains largely open. For hardening composites, the RVE size was found in Gitman et al. (2007) to be generally larger than for linear elastic case, and not to exist for softening materials. For a perfectly plastic porous matrix, strain localization occurs in the form of slip band networks as shown for instance by Besson (2004), Bilger et al. (2005, 2007). Finer discretization may lead to even thinner band structures. However the overall stress state is generally found to be mesh–independent and to converge when the volume element size is increased. In Ghosh et al. (2009), population of holes and inclusions are considered within an elastic–plastic damaging matrix described by a GTN model. The question of RVE size is tackled there from the point of view of statistical distributions of holes and inclusions.

In this contribution a systematic study of the macroscopic constitutive response of porous metals is performed based on Monte Carlo type numerical simulations. The focus is on three-dimensional microstructures constructed using a periodic assemblage of hard core spheres representing the voids. The aim of the numerical study is the comparison of some of the existing analytical models to the numerical results obtained from finite element computations. Surprisingly, such a comparison has not been carried out in a systematic manner yet in the literature and can provide essential prediction for the design of a overall constitutive model that fits closely to the volume element simulations, as done in this work. In contrast to many previous contributions, pore volume fractions up to 30% are investigated in order to examine the efficiency of the analytical estimates. Such porosities can be found for instance in the case of some metallic foams at intermediate volume fractions like aluminum and titanium foams produced by entrapped gas expansion for which pores are still isolated in the metal matrix (Gibson and Ashby, 1997). Other examples for materials exhibiting intermediate or large porosities are given by geomaterials such as sandstone or closed cell polymer foams with nearly incompressible matrix. While these materials are not in the scope of the current investigation, the presented results can be considered as a preliminary investigation towards a treatment of such materials. Notably, the performed simulations can account for the complex mechanical interactions due to the geometry and the physical nonlinearity of the material. These interactions are assumed to have a non-negligible influence on the effective material response (see also Bilger et al., 2005, 2007).

The paper is organized as follows. In Section 2 the constitutive assumptions on the micro-heterogeneous material are formulated and the generation and discretization of the periodic unit cells is described. Additionally, the statistical properties of the microstructures are evaluated using different statistical descriptors in order to assess the morphological and topological representativeness of the considered ensembles. The convergence of the macroscopic response with respect to the spatial discretization is analyzed in a mesh density study. The asymptotic stress response of the more than 500 investigated unit cell computations is presented in Section 3. The physical representativeness of the computational results is validated by variation of the number of pores and the type of boundary conditions. Moreover, the local plastic strain fields are discussed and the observations are related to the ones made by Bilger et al. (2005). In Section 4 a comparison with analytical approaches is performed and a modified GTN model is proposed. The latter incorporates only one additional parameter, although the new criterion is able to capture all of the computed points to an excellent extent.

2. Modeling

2.1. Constitutive assumptions

In the following we are concerned with the macroscopic behavior of isotropic porous metals. The Young's modulus $E = 200$ GPa and the Poisson ratio $\nu = 0.3$ are assumed. Inelastic incompressibility is asserted and an isotropic von Mises J_2-type plasticity model with constant yield stress $\sigma_F = 100$ MPa is used. No hardening is considered in order to be able to relate the obtained results to the ones predicted by existing micromechanical models in Section 4. The consideration of path-dependent plasticity and of the elastic deformation of the material is a noteworthy difference with respect to existing literature where only few authors have accounted for these effects (e.g. Ghosh et al., 2009). For example the computational investigations by Bilger et al. (2005, 2007) are based on deformation theory, i.e. they do not consider the local path-dependency of the constitutive response. Furthermore a proportional loading is assumed.

A geometrically linear description is employed to allow comparison with existing analytical models which are valid in the linear setting only. The infinitesimal strain tensor ε is defined as the symmetric part of the gradient of the displacement field $\boldsymbol{u}$. The Cauchy stress tensor is denoted $\boldsymbol{\sigma}$. The pores with the spherical boundary $\mathscr{P}$ are assumed to be pressure free. More specifically, the surface of the pores is a free boundary and the traction vector $\boldsymbol{t} = \boldsymbol{\sigma}\boldsymbol{n}$ is zero on $\mathscr{P}$, where $\boldsymbol{n}$ denotes the unit normal pointing out of the pores. Note that in the given geometrically linear setting the evolution of the porosity due to applied loading cannot be attributed for.

A two-scale material is assumed with the smaller scale denoting the level at which individual pores are observed and the larger scale the structural level at which an effective (unknown) behavior is observed. The considered unit cell Ω_{tot} is taken as a cube in which the matrix $\Omega \subsetneq \Omega_{\text{tot}}$ and the voids $\Omega_{\text{tot}} \backslash \Omega$ are placed. The two scales are assumed to be clearly separated for usual homogenization theory to apply. The displacement field is assumed zero within the voids. In the given setting the microscopic and macroscopic stress and strain tensors are related by (see, e.g., Nemat-Nasser and Hori, 1999)

$$\bar{\varepsilon} = \frac{1}{|\Omega_{\text{tot}}|}\int_{\Omega} \varepsilon \mathrm{d}V + \bar{\varepsilon}_{\text{c}} = (1-f)\langle\varepsilon\rangle_{\Omega} + \bar{\varepsilon}_{\text{c}}, \quad \bar{\varepsilon}_{\text{c}} = \frac{1}{|\Omega_{\text{tot}}|}\int_{\mathscr{P}} \operatorname{sym}(\boldsymbol{u}\otimes\boldsymbol{n})\mathrm{d}A, \tag{1}$$

$$\bar{\boldsymbol{\sigma}} = \frac{1}{|\Omega_{\text{tot}}|}\int_{\Omega} \boldsymbol{\sigma}\mathrm{d}V = (1-f)\langle\boldsymbol{\sigma}\rangle_{\Omega}, \tag{2}$$

where $\bar{\varepsilon}_{\text{c}}$ represents the cavity strain due to the deformation of the boundary of the pores and f denotes the pore volume fraction.

2.2. Microstructure generation

In the following periodic aggregates consisting of a voided homogeneous material are considered. Attention is confined to spherical non-overlapping pores with constant radius R, i.e., a single size population of spheres is investigated. The number of spheres within the cuboidal unit cell is denoted N. The pore volume fraction f is related to the other parameters via

$$f = \frac{4\pi N R^3}{3|\Omega_{\text{tot}}|}, \tag{3}$$

where $|\Omega_{\text{tot}}|$ is the volume of the considered unit cell.

In order to generate the pore distribution for given f and N, a Poisson point process is used. It provides the center points of the voids based on the principle of random sequential addition. A minimum distance of the non-overlapping spheres of 2.5% of the diameter was enforced in order to allow for an adequate spatial discretization. The periodicity of the pore distribution was enforced by copying all pore centers 26 times around the cuboidal cell. In order to be able to average out effects due to the individual realization of the microstructures, a Monte Carlo type statistical approach is pursued with N_r realizations for each tuple (f, N). The examined values for f and N are listed in Table 1 together with the number of realizations computed. The choice for the numbers of realizations is motivated in Section 3.2. Examples for different pore volume fractions are presented in Fig. 1.

The meshing tool Netgen (Schöberl, 1997) was used to produce periodic spatial discretizations at high quality. Ten node second-order tetrahedral elements were used to avoid volume locking which is very pronounced for the investigated examples when using linear tetrahedra. The quality of the mesh is gradually improved by Netgen over several mesh sweeps and an excellent quality of the discretization was observed. The smallest investigated pore fraction of 0.1% can be considered as almost dilute. Hence, a single pore embedded in a cuboid is also considered as a reference case for comparison with literature results. The results of the random microstructures are related to the ones obtained from the single-pore model to justify the reduced value of $N = 20$ for the smaller volume fractions. For the highest volume fraction ($f = 30\%$) the same was done to verify that the single-pore model is not sufficient. In Fig. 2 discretizations at 0.1, 1, 10 and 30% volume fraction are shown with the mesh density used in the statistical studies. For the lowest volume fraction the mesh in the calculations included up to more than one million degrees of freedom in the presented investigations.

In order to show convergence with respect to the mesh size and in order to investigate the error with respect to the finite-dimensional approximation of the solution space, a mesh convergence study was performed based on an ensemble containing 10 pores and 10% of porosity. Six different discretization levels have been considered, where Table 2 provides the number of degrees of freedom and the number of elements. Three of the discretizations are shown in Fig. 3.

2.3. Boundary conditions

The interest in this work is the investigation of varying stress triaxiality ratios in order to assess the pressure dependency of the macroscopic yield surface of the porous material. Due to the constant yield stress on the small scale, stress-driven boundary conditions, i.e., anti-periodic traction boundary conditions, have not been pursued due to the delicate assessment of admissible load increments. The use of purely kinematic boundary conditions is generally possible in terms of prescribed strains and a periodic displacement fluctuation field. However, such kinematic conditions imply that the structure of the stress tensor is a priori unknown, i.e. macroscopic shear stress components are likely to be found for uni-axial elongation etc. Therefore, the stress triaxiality can only be estimated before-hand. In order to induce varying stress triaxiality without constraining the deformation of the material too much, it was decided on mixed periodic boundary conditions. A varying overall triaxiality results from the prescription of the real valued parameters α, β. For the simulation time t the boundary conditions are

$$\left.\begin{aligned} \bar{\varepsilon}_{11}(t) &= t\dot{\varepsilon}_0(\alpha+\beta),\\ \bar{\varepsilon}_{22}(t) &= t\dot{\varepsilon}_0(-\alpha+\beta),\\ \bar{\varepsilon}_{33}(t) &= t\dot{\varepsilon}_0\beta,\\ \bar{\sigma}_{12}(t) = \bar{\sigma}_{13}(t) &= \bar{\sigma}_{23}(t) = 0. \end{aligned}\right\} \tag{4}$$

Here $\dot{\varepsilon}_0 > 0$ is a prescribed reference deformation rate. These conditions are numerically realized by imposing only the mean of the normal displacements on the surface of the unit cell and periodic displacement fluctuations. Under the given loading the mean shear tractions on the surfaces vanish and, hence, the shear components of the macroscopic stress tensor are always zero. Thus, the von Mises stress and the hydrostatic stress depend only on the diagonal components of the macroscopic stress $\bar{\boldsymbol{\sigma}}$ according to

$$\Sigma_{\text{eq}} = \sqrt{\frac{3}{2}}\|\bar{\boldsymbol{\sigma}}'\|_2 = \sqrt{\frac{(\Sigma_{xx}-\Sigma_{yy})^2 + (\Sigma_{xx}-\Sigma_{zz})^2 + (\Sigma_{yy}-\Sigma_{zz})^2}{2}}, \tag{5}$$

$$\Sigma_{\text{m}} = \frac{1}{3}\text{tr}(\bar{\boldsymbol{\sigma}}) = \frac{\Sigma_{xx}+\Sigma_{yy}+\Sigma_{xx}}{3}, \tag{6}$$

Table 1
Overview of the examined microstructures.

f	0.1%	1%	2.5%	5%	10%	20%	30%
N	20	20	20	20	50	50	50
N_r	5	5	10	10	10	10	10

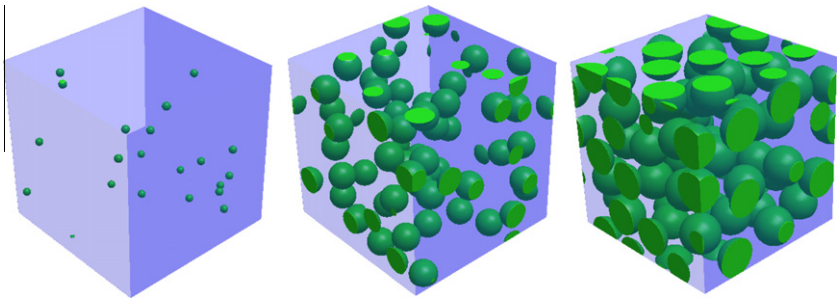

Fig. 1. Realizations of microstructures at pore volume fractions of 0.1% (left), 10% (middle) and 30% (right).

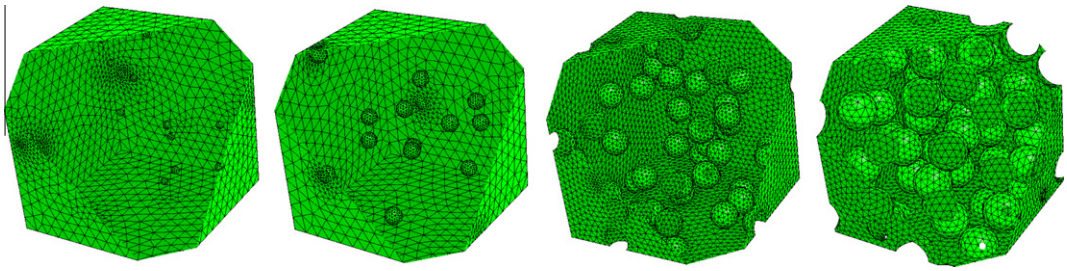

Fig. 2. Discretizations of microstructures containing 0.1, 1, 10 and 30% of pores as used in the statistical studies.

Table 2
Different mesh refinement levels for the mesh density study ($N = 10, f = 10\%$).

Level	h_1	h_2	h_3	h_4	h_5	h_6
# Degrees of freedom	22,389	47,982	121,848	319,005	1,274,298	3,467,112
# Elements	4,127	8,940	26,533	71,038	296,229	853,927

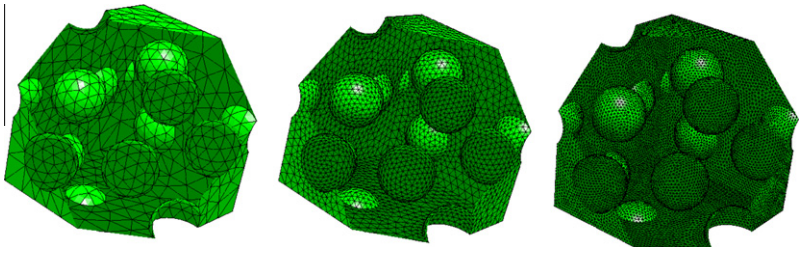

Fig. 3. Discretizations at refinement level h_1, h_4 and h_6 (left to right).

where $\bar{\boldsymbol{\sigma}}'$ denotes the deviatoric part of $\bar{\boldsymbol{\sigma}}$. The two stress measures are defined implicitly by the mixed conditions, i.e. without direct control of the triaxiality parameter. Due to the chosen mixed loading the two stress measures contain only three independent parameters. Therefore, the control on the triaxiality is improved over purely kinematic loading for computationally affordable unit cells, i.e., for a finite number of pores. The nine different tuples (α_i, β_i) examined in the following are given in Table 3. Alternative stress-based loading conditions are often used to control the triaxiality ratio during loading (see, e.g., Besson, 2004). However, for more than 500 simulations as considered in this work we have preferred the previous mixed periodic boundary conditions due to its computational robustness.

In the finite element simulations the periodicity of the displacement field was enforced using a linear relation between the displacement of the master and slave nodes on the surface of the unit cell. A parallel self-written finite element implementation was used to solve the physically nonlinear problem. Excellent numerical performance was achieved using the iterative solver HIPS (http://hips.gforge.inria.fr) for the large linear systems obtained from the discretization of the linearized constitutive equations. An implicit time integration procedure based on a backward Euler scheme was used. Due to the absence of hardening, convergence was hard to attain in all computations. A reason for this is found in the lack of strong ellipticity of the incremental Gibbs potential associated with the material law due to the lack of isotropic hardening. A line search

Table 3
Load parameters α, β used in the simulations.

i	1	2	3	4	5	6	7	8	9
α_i	1.00	1.00	1.00	1.00	1.00	1.00	1.00	0.50	0.00
β_i	0.00	0.05	0.10	0.15	0.25	0.50	1.00	1.00	1.00

procedure incorporating the Armijo rule was found to improve the numerical performance significantly, or to allow for convergence at all. This holds particularly true for the very small pore fractions which result in largely fluctuating stress, strain and displacement fields due to the high curvature on the pore boundaries. Two computations resulted in poor convergence for the two smallest pore volume fractions and did not terminate. The respective results were not considered in the subsequent investigations. However, the good agreement to the single pore model shows, that the additional contribution due to multiple pores is negligible at such small porosities. The path-dependency of the solution is accounted for by a sufficiently fine discretization of the problem with respect to the simulation time.

2.4. Statistical properties of the microstructures

As stated earlier, the representativeness of the microstructure can be subdivided into two conditions: First, the morphology and the topology of samples have to be representative. This is a necessary but not a sufficient condition which is examined in the following. The representativeness of the computational results obtained from microstructures satisfying this requirement are analyzed in Section 3.2. Three different statistical properties of the microstructures have been analyzed in order to examine the geometric representativeness of the obtained results: (i) the existence of pore clusters, (ii) the k-nearest neighbor distance and (iii) the two-point correlation of the pores. The first two conditions are directly related to the pore–pore neighbor relations and the third can be used as an indicator for the isotropy of the micro structure.

The assessment of the representativeness of the microstructures is required due to the finite size of computationally feasible unit cells, although analytical results concerning the statistics of infinite structures for hard core models of spheres exist (see e.g. Torquato, 2002). Notably the statistical tools used for the analysis have to account for the periodicity of the unit cell, which is rarely the case in commercial programs.

For the detection of pore clusters the algorithm used, e.g., by Bilger et al. (2005) was employed. In order to find pore clusters, the radius of the non-overlapping spherical pores is artificially augmented by a positive offset δR. Based on a collision detection algorithm chains of interconnected pores are then identified. The procedure is illustrated in Fig. 4. It was found that none of the microstructures showed pronounced clustering. However, almost all microstructures show micro-clusters consisting of 2 or 3 pores very close to each other (Fig. 5). It is thus expected that clustering has negligible effects on the constitutive response which are not subject of the current investigation. For a detailed study investigating these effects it is referred to Bilger et al. (2005, 2007). Note also that for higher porosities it is not possible to distinguish between clusters as the distance between neighboring pores is always very small.

In order to analyze the average pore neighbor relationship of the microstructure in more detail, we introduce for the pore indexed i the k-nearest neighbor distance d_k^i as the minimum distance at which k neighbors are found ($1 \leqslant k < N$). The distribution of d_k^i can then be compared between different realizations to judge on the representativeness of the structure. Therefore the average value $\bar{d}_k$ over all pores and the standard deviation $\sigma(d_k)$ are compared for different realizations of the microstructures. Other values of interest are the extremal magnitudes (min./max.) of d_k over all pores. In Fig. 6 the average value $\bar{d}_k$ is plotted for five realizations at different volume fractions (lines), where d_k is given as a non-dimensional value with respect to the length of an edge of the unit cell. Additionally, the minima and maxima are shown (squares and dots) and the $\pm 3\sigma(d_k)$ confidence interval is indicated in terms of dashed lines. For all volume fractions it is found that both the mean value and the standard deviation of d_k vary only slightly. However, some fluctuation in the minima and maxima is found. Nevertheless, these fluctuations can be considered negligible. The results obtained for the other than the four shown volume

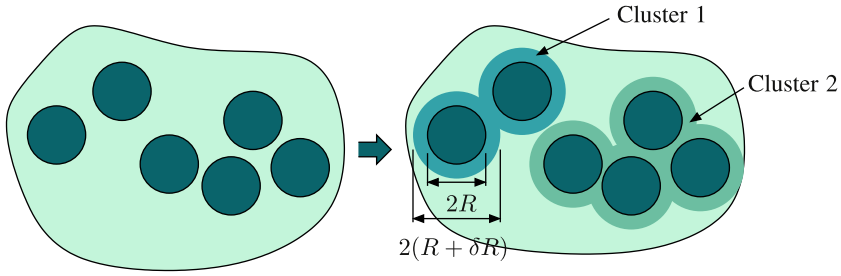

Fig. 4. Schematic illustration of the pore cluster identification algorithm (two-dimensional case).

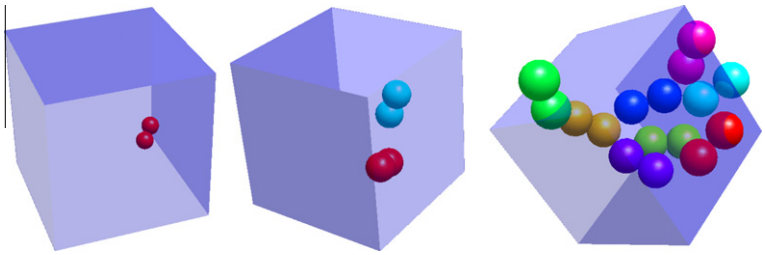

Fig. 5. Pore clusters for $f = 1\%$, $N = 20(\delta R = 0.3R$, left), $f = 5\%$, $N = 20(\delta R = 0.2R$, middle), $f = 30\%$, $N = 50$ ($\delta R = 0.1R$, right); all shown pore clusters consist of 2 pores, except one at $f = 30\%$ (3 pores).

fractions are omitted for brevity. They show the same qualitative results. Due to the presented results the microstructures can be considered to show similar pore–pore neighbor relations.

The third statistical tool used to evaluate the properties of the microstructure is the two-point autocorrelation function of the pores. An algorithm based on geometrically exact intersection of spheres was developed and implemented into a C++ program. Multi-threading was used to reduce the computational time on shared memory multi-processor systems and near optimal speed-up was achieved. The autocorrelation function is plotted in Fig. 7 for two microstructures. It is found that the two-point function is almost directionally independent, i.e. nearly isotropic. As is known for models of non-overlapping circles and spheres, a region around the objects exists in which the two-point function is smaller than the asymptotic value f^2 at infinity. This property was also found for the examined microstructures.

2.5. Mesh density convergence study

In order to assure a sufficient quality of the presented results with respect to the spatial resolution, a convergence study has been performed on a unit cell for the parameters $f = 10\%$, $N = 10$. The load case $\alpha = 1$, $\beta = 0$ was chosen as an example. The finest solution was taken as reference and the response of the other discretizations is related to the last calculated value of this discretization in Fig. 8. The error with respect to the spatial discretization is found to decrease monotonically and the

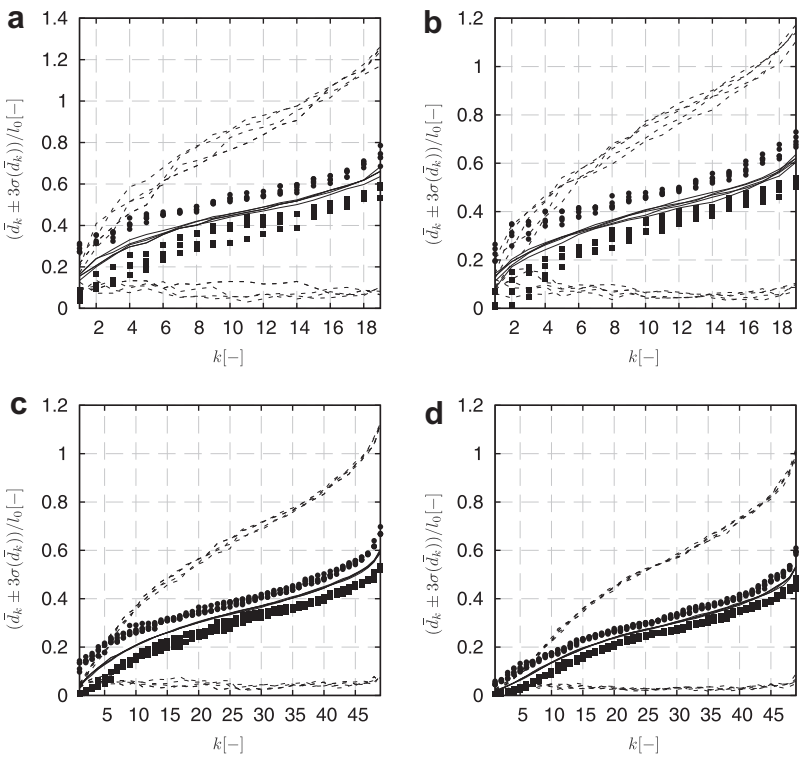

Fig. 6. Average k-nearest distance of the pores for 0.1% (a), 1% (b), 10% (c) and 30% (d) pore volume fraction; 5 realizations with min./max. values (points), $k = 1,\ldots,19$ (a,b) and $k = 1,\ldots,50$ (c,d); dashed lines: 3σ confidence interval (values normalized with respect to the edge length of the unit cell l_0).

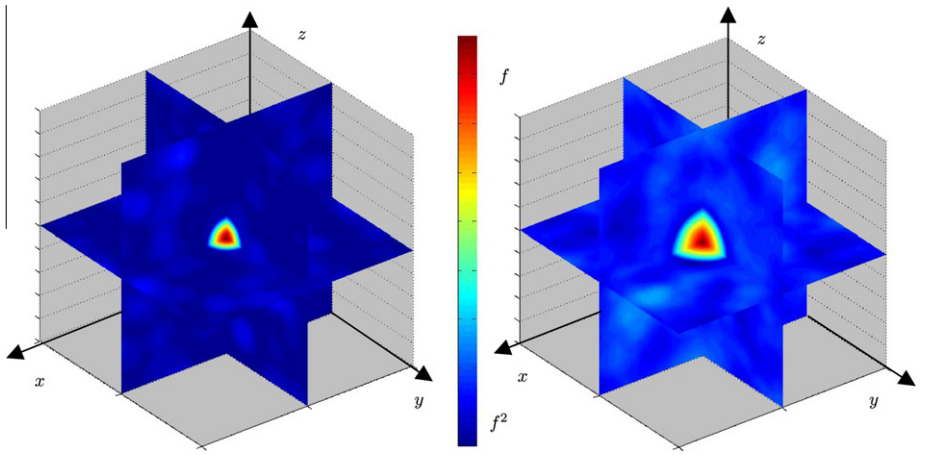

Fig. 7. Two-point autocorrelation of the pores for $f = 1\%$ (left) and $f = 10\%$ (right).

difference between two successive refinement levels tends to zero. The observed small hydrostatic stress is due to the small number of inclusions and should vanish under the given pure shear load for a large number of pores due to the isotropy of the aggregate. The relative errors with respect to the number of degrees of freedom is represented in Table 4.

Based on this study a medium mesh density was chosen for the statistical studies. Moreover, on the basis of the convergence study the error for the used discretizations is considered small with respect to other influence factors, such as the variation of the micro-structural geometry between different realizations. It should be noted that the width of the plastic zone is to some extent mesh dependent which is a known result from limit analysis in ideally plastic materials. However, Fig. 8 and Table 4 show the convergence of the macroscopic stress response which is the focus of the present study.

3. Computational results

3.1. Asymptotic results

The asymptotic behavior of the porous microstructures is subject of the present investigation. In order to approximate the asymptotic response of the porous medium, the macroscopic stress at the end of the simulation time is used. It was verified that all of the taken values are stationary in the sense that the change in the macroscopic stress tends to zero when the overall strain loading is increased. In order to do so, the macroscopic von Mises equivalent and hydrostatic stress are plotted versus the non-dimensional loading time in Fig. 9. It is found that the stresses are stationary at the end of the simulations. This holds true for all examined microstructures.

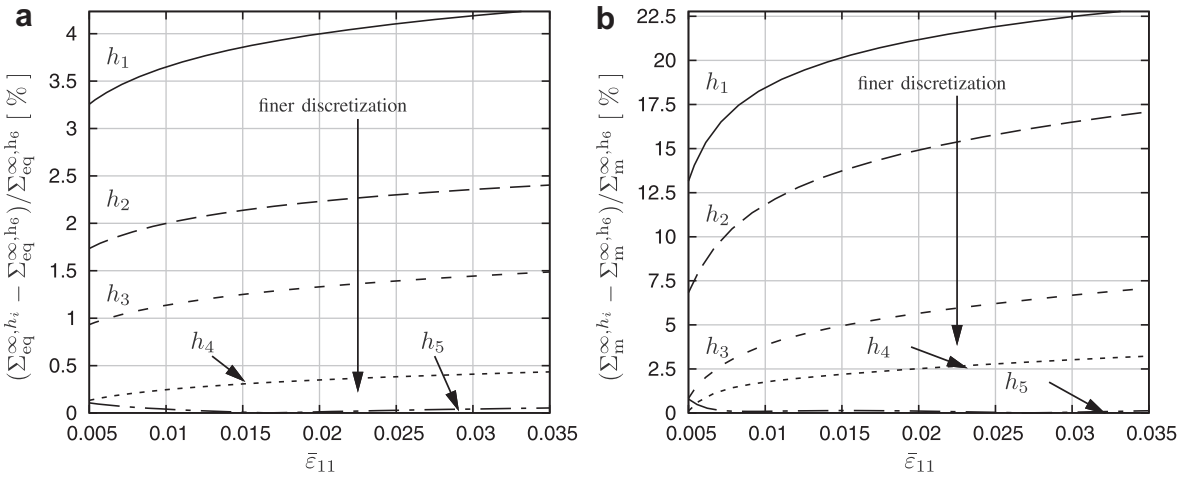

Fig. 8. Relative error with respect to the asymptotic von Mises equivalent stress (a) and asymptotic effective hydrostatic stress (b) for the discretizations $h_1, \ldots, h_5$ (asymptotic value of the finest discretization taken as reference).

Table 4
Relative error of the mesh density study with respect to the finest discretization.

# DOF	22,389	47,982	121,848	319,005	1,274,298	3,467,112
$\frac{\Sigma_{eq}^{\infty,h_i}-\Sigma_{eq}^{\infty,h_6}}{\Sigma_{eq}^{\infty,h_6}}$ [%]	1.137	0.855	0.357	0.164	0.008	reference
$\frac{\Sigma_{m}^{\infty,h_i}-\Sigma_{m}^{\infty,h_6}}{\Sigma_{eq}^{\infty,h_6}}$ [%]	4.290	2.424	1.507	0.444	0.058	reference

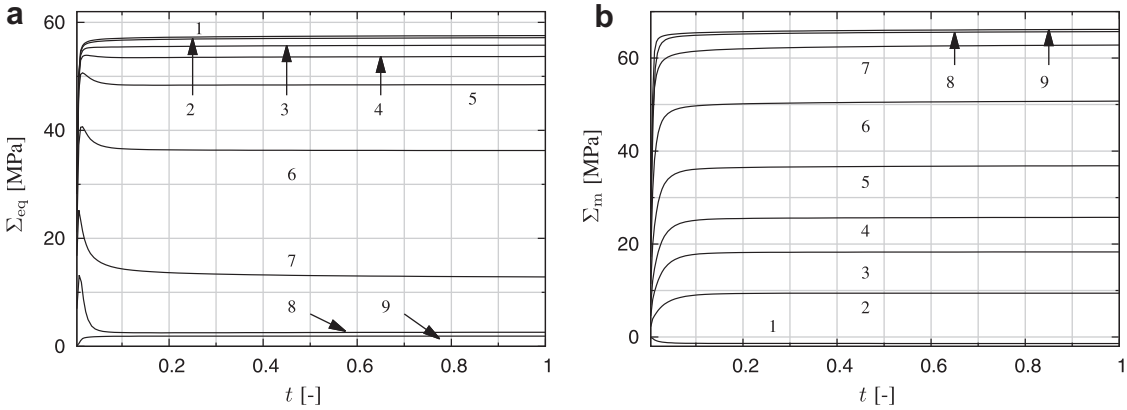

Fig. 9. Effective von Mises equivalent stress (a) and hydrostatic stress (b) versus non-dimensional loading time for one realization at $f = 30\%$ for the nine considered load cases (numbers indicate the load cases listed in Table 3).

The asymptotic behavior is plotted in the stress space (Σ_{eq} vs. Σ_m) in Fig. 10 for all examined microstructures and all nine considered loading directions. The results of the single pore model for $f = 0.1\%$ and 30% are also shown. The computed data can be used to compare analytic models to simulation data and to identify parameters for phenomenological approaches (see Section 4).

3.2. Representativeness of the results

The geometrical properties of the used unit cells are analyzed in Section 2.4. In this section the mechanical representativeness of the computational results is assessed. The latter can be considered as a sufficient condition that has to be satisfied in addition to the geometrical representativeness. By comparison of the single pore models and the random microstructures in Fig. 10 it can be concluded that for the dilute limit $f \to 0\%$, a single pore in a reference cell appears to give a sufficiently close approximation of the ductile behavior of the examined random isotropic microstructures. This is not the case for the

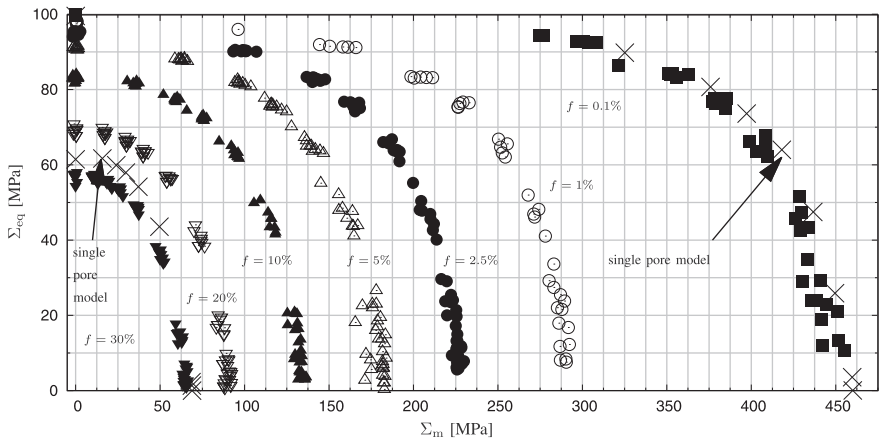

Fig. 10. Calculated asymptotic stress response of the porous microstructures for pore volume fractions from 0.1 to 30%; the single-pore model is shown for comparison at $f = 0.1\%$ and 30%.

higher volume fractions. The asymptotic stress response of the examined microstructures at 30% pore volume fraction including 50 pores each shows a deviation of more than 10% from the single pore model.

In order to verify that the results obtained from the random microstructures defined by Table 1 are representative for the different volume fractions, the following points have been investigated: (i) convergence with respect to the size of the unit cell, (ii) convergence with respect to the type of boundary condition, and (iii) convergence with respect to the ensemble average of the Monte Carlo study. For the latter, the asymptotic stresses obtained from the statistical study at a porosity of 20% and using 50 pores are examined closely for the loading path characterized by $\alpha = 1$, $\beta = 0.25$. The latter was chosen because it shows both, pronounced deviatoric and hydrostatic stress components.

In the considered Cauchy continuum framework no length scale exists. Thus the size of the unit cell is given by the number of pores N which should be chosen large enough. In order to examine the influence of the latter, a new set of random microstructures was created and discretized for the porosity $f = 20\%$ and varying number of pores ($N \in \{5, 10, 20, 50, 75, 100, 150, 200\}$). All these microstructures are subjected to the indicated loading path and the asymptotic stresses are analyzed. In addition to the periodic boundary conditions described before, kinematic uniform boundary conditions were applied to identical cells in order to account for the second aspect. The latter was done for two reasons. First, the effective response of a material subjected to the same loading (here: same macroscopic strain) should be independent of type of boundary condition which is intrinsically unknown in real applications. Second, it is a known result that the uniform kinematic boundary conditions represent an upper bound for the effective response in an energetic sense (e.g. Sab and Nedjar, 2005, Ranganathan and Ostoja-Starzewski, 2008). A minor modification was necessary in the sense that the entire displacement on the boundary was prescribed which slightly differs from the mixed periodic boundary conditions described in Section 2.3. It was verified that both, the effective shear stresses with kinematic uniform boundary conditions and the effective shear strains with periodic boundary conditions are close to zero, i.e. that the influence of this difference can be considered negligible. In order to guarantee independence of the fluctuations with respect to the chosen spatial discretization, rather fine meshes with up to one million degrees of freedom are used.

The asymptotic hydrostatic and equivalent stress response are shown in Fig. 11. As expected, the difference between the two different loading conditions for the same realization is rather pronounced (box and circles) for small unit cells, i.e. at low number of pores. This does particularly hold true for the hydrostatic part of the stress (Fig. 11, right). For higher number of pores the differences due to the boundary condition reduce significantly.

Moreover, the average value obtained from the ten different computations of the statistical study at $N = 50$ is plotted in terms of a dashed line and the confidence interval of the statistical study given by plus/minus the standard deviation is indicated in gray. Notably, all computed points with periodic boundary conditions are found within or close to this range. Within the realizations containing 50 voids the largest deviations from the mean value of the 10 simulations are 4% for the pressure and 1.6% for the von Mises stress. However, the standard deviation of both values is approximately half of this error. Additionally, the asymptotic values for periodic boundary data for the largest unit cell ($N = 200$) do almost coincide with the averages from the statistical investigation. More precisely, the realizations containing 150 or 200 pores show a deviation of less than 1% in the von Mises equivalent stress and 2% in the hydrostatic stress from this line. Interestingly, the effective von

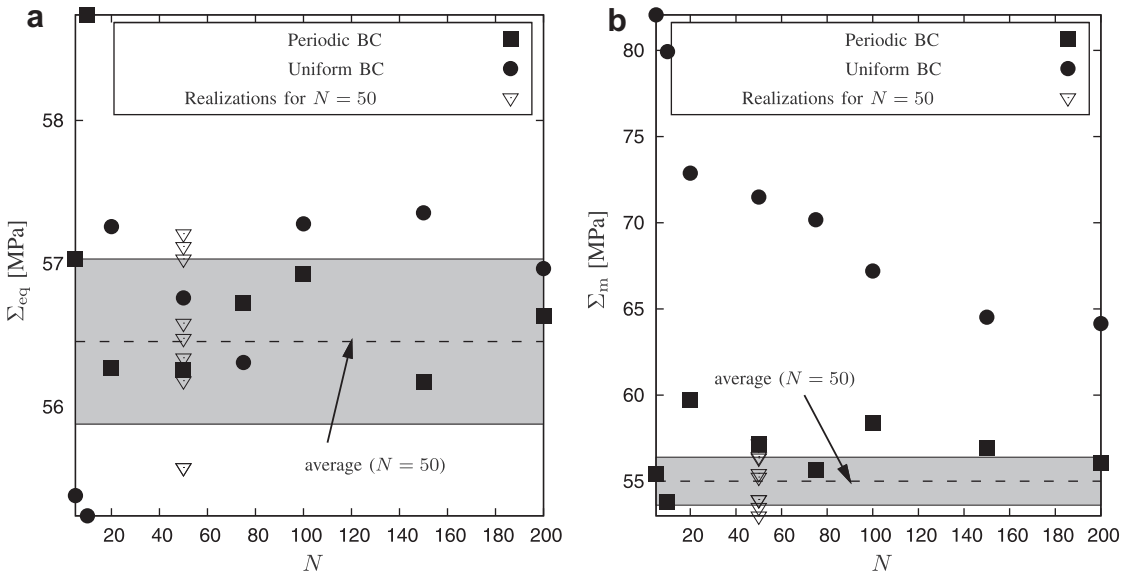

Fig. 11. Comparison of the asymptotic von Mises equivalent stress (a) and hydrostatic stress (b) for different numbers of pores and boundary conditions; the values of the statistical study are also shown (gray area: $\pm\sigma(\Sigma_{eq})$ and $\pm\sigma(\Sigma_m)$).

Mises equivalent stress for the uniform boundary conditions is rather close to the solution obtained for the periodic displacement fluctuation boundary conditions. However, the hydrostatic stress is grossly overestimated.

Surprisingly some of the effective stress responses of the UKBC appear to be softer than for the PKBC, see for instance Σ_{eq} for $N = 5$ or $N = 10$, although they are known to provide an upper bound for the PKBC. This is due to the fact that the bounding character is not found in terms of the stresses, but in terms of the work per unit volume needed to attain the final prescribed macroscopic deformation. The latter is computed for the time interval $[0,T]$ by virtue of the Hill-Mandel condition

$$\overline{W}_{\mathrm{tot}} = \int_0^T \langle \boldsymbol{\sigma} \cdot \dot{\varepsilon} \rangle \mathrm{d}t = \int_0^T \bar{\boldsymbol{\sigma}} \cdot \dot{\bar{\varepsilon}} \mathrm{d}t. \tag{7}$$

The total work has been calculated for both types of boundary conditions and for all considered values of N in Fig. 12. While the values found for the periodic solutions are almost identical for all values of N, i.e., even for $N = 5$, the uniform boundary conditions show significantly higher values. This can be interpreted in the sense that the total work expended on the unit cell is nearly invariant with respect to the actual unit cell size for PKBC. Further, it is found that for homogeneous displacements prescribed on the boundary the energy is decreasing with rising N. The results plotted in Fig. 12 clearly show that the UKBC solution tends to the PKBC solution.

Concerning the number of realizations N_{r} for each of the pore volume fractions an approach based on the relative error estimator for a random variable Z as provided in Kanit et al. (2006) is chosen based on the standard deviation $\sigma(Z)$ and the mean value $\overline{Z}$ according to

$$\epsilon_{\mathrm{rel}}(Z) = \frac{2\sigma(Z)}{\sqrt{N_{\mathrm{r}}}\overline{Z}}. \tag{8}$$

Here two different variables are observed in each calculation: the hydrostatic stress Σ_{m} and the von Mises stress Σ_{eq}. For certain loadings either one of these variables is close to zero and a relative error with respect to this mean value is not a straight-forward choice. Based on a modified normalization condition, the following two relative errors are examined

$$\tilde{\epsilon}_{\mathrm{eq}} = \frac{2\sigma(\Sigma_{\mathrm{eq}})}{\sqrt{N_{\mathrm{r}}}\sqrt{\overline{\Sigma}^2_{\mathrm{m}} + \overline{\Sigma}^2_{\mathrm{eq}}}}, \quad \tilde{\epsilon}_{\mathrm{m}} = \frac{2\sigma(\Sigma_{\mathrm{m}})}{\sqrt{N_{\mathrm{r}}}\sqrt{\overline{\Sigma}^2_{\mathrm{m}} + \overline{\Sigma}^2_{\mathrm{eq}}}}. \tag{9}$$

These errors have been evaluated for all pore volume fractions for each of the nine loadings of Table 3 and by taking into account the number of realizations (see Table 1). It has been verified that $\tilde{\epsilon}_{\mathrm{eq}}$ is smaller than 2% for all calculations and that $\tilde{\epsilon}_{\mathrm{m}}$ is smaller than 2.2% except for $f = 0.1\%$ and $f = 1\%$ for the load parameters $\alpha = 1$, $\beta = 0.05$ where $\tilde{\epsilon}_{\mathrm{m}}$ was still smaller than 3.5%.

In addition to the analysis of the effective stress response and the expended work, the local plastic strain fields are also analyzed. For $N = 5$ (Fig. 13) and $N = 200$ (Fig. 14) the computed equivalent plastic strain at the end of the simulation is compared. On the left hand side the uniform boundary conditions are shown, on the right hand side the field obtained using periodic displacement fluctuations is plotted. For a small number of pores the plastic strain fields are largely different for the two types of loading. For $N = 200$ the effect is limited to a boundary close region, i.e., the plastic strain found close to the surface is significantly different. However, the fields found inside of the cell show an excellent agreement. This leads to the conclusion that for an infinite cell size the two solutions are expected to coincide almost everywhere with respect to the Borel–Lebesgue

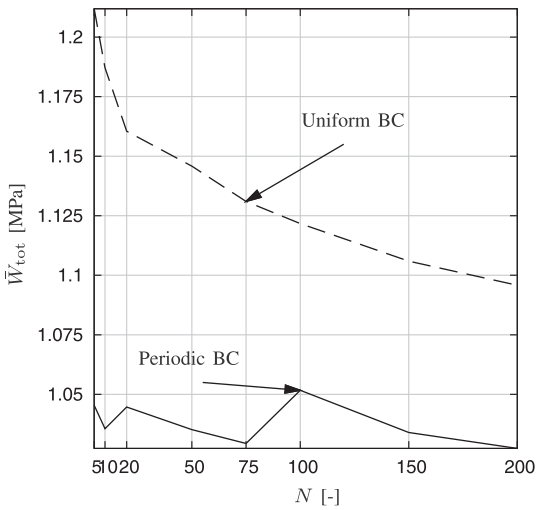

Fig. 12. Comparison of the work density $\overline{W}_{\mathrm{tot}}$ needed to attain the prescribed deformation for uniform kinematic boundary conditions and periodic fluctuation fields.

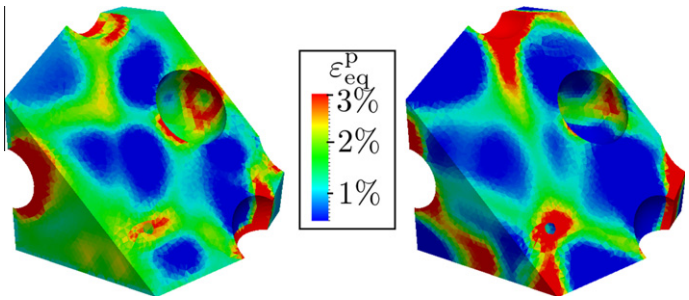

Fig. 13. Accumulated plastic strain for UKBC (left) and PKBC (right) at the final prescribed loading for the microstructure containing 5 pores.

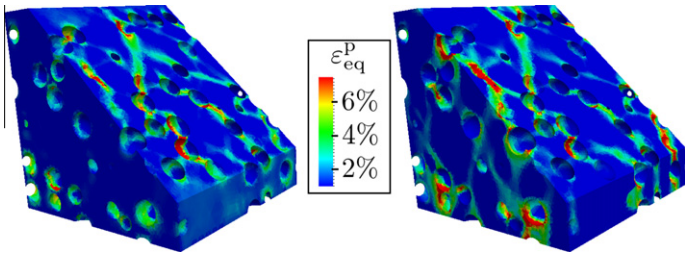

Fig. 14. Accumulated plastic strain for UKBC (left) and PKBC (right) at the final prescribed loading for the microstructure containing 200 pores.

measure. Moreover the discrepancies still observed for 200 pores show that the needed cell size to attain this result is presumingly very large, i.e. it involves thousands of spherical voids. The mentioned results show that the computational results presented earlier can be considered representative for the considered microstructural class.

3.3. Lode angle

It is known that the stress triaxiality classically referred to by the ratio of equivalent stress and mean stress does not suffice to depict the actual material behavior. It is known that for isotropic viscoplastic polycrystals the third invariant of the stress can influence the effective constitutive response (Böhlke, 2004). For porous materials, investigations by Kim et al. (2004), Danas et al. (2008) and others have addressed this topic explicitly. Usually the third invariant is considered in the context of the Lode angle. Although not scope of the current investigation the influence of the third invariant should be eliminated from the presented results. Therefore we have evaluated the Lode angle for the different realizations undergoing the same loading. As an example the mean and the standard deviation for $f = 10\%$ are given in Table 5 for the nine different load case. In Table 6 the Lode angle is analyzed for the seven different porosities undergoing the same loading. The small fluctuations found confirm the choice of mixed boundary conditions.

In order to show that these fluctuations have minor impact on the results we relate them also to the results of Danas et al. (2008) (see Fig. 3). These results were obtained by a second order method for $f = 10\%$ and a rate sensitivity parameter $m = 0.1$. For zero applied mean stress (Fig. 3.a) close to no fluctuations are found. For an applied stress state close to pure hydrostatic load (Fig. 3.b) it is found that the minimum and maximum values of the second order estimate of the ratio $\Sigma_{\mathrm{eq}}/\sigma_{\mathrm{F}}$ vary approximately between 0.0875 and 0.10 equaling a variation of approximately ±6%. For small variations in the Lode angle the variations in the pressure dependency is predicted to be even smaller. Hence, the variations in the Lode angle in our computations can be considered to have negligible influence on the overall results. It should also be noted that the observed Lode angles (typically around 35–40°) coincide approximately to the mean value of the gauge function in Fig. 3.b in Danas et al. (2008).

3.4. Local plastic strain fields

The distribution of the accumulated plastic strain field has been analyzed for different loading conditions and microstructures. Perfectly plastic, i.e. non-hardening, metals tend to form strongly localizing bands. For instance, Bilger et al. (2005) reported a pronounced influence of the applied hydrostatic load on the dispersion and curvature of the localization zones of the plastic deformation for periodic unit cells containing 39 pores at a volume fraction of 0.6%. The results of our study confirm these observations for all examined volume fractions, see for instance Fig. 15.

In addition it was found that for the higher volume fractions the plastic strain tends to be more diffuse than for the small volume fractions. The resulting patterns are complex due to the small distance between neighboring pores with respect to

Table 5
Mean Lode angle θ and its standard deviation for the nine load cases for a porosity of 10%.

α_i	1.00	1.00	1.00	1.00	1.00	1.00	1.00	0.50	1.00
β_i	0.00	0.05	0.10	0.15	0.25	0.50	1.00	1.00	1.00
θ	30.1°	38.3°	39.9°	41.1°	43.2°	48.2°	46.5°	33.5°	31.2°
$\sigma(\theta)$	0.21°	1.75°	1.74°	1.78°	2.19°	4.45°	8.46°	12.9°	13.2°

Table 6
Mean Lode angle and its standard deviation for $\alpha = 1.00$, $\beta = 0.10$ for all considered porosities.

f	0.1%	1%	2.5%	5%	10%	20%	30%
θ	39.3°	37.7°	37.9°	37.7°	39.9°	38.5°	39.1°
$\sigma(\theta)$	2.09°	3.65°	2.30°	1.25°	1.74°	1.50°	2.16°

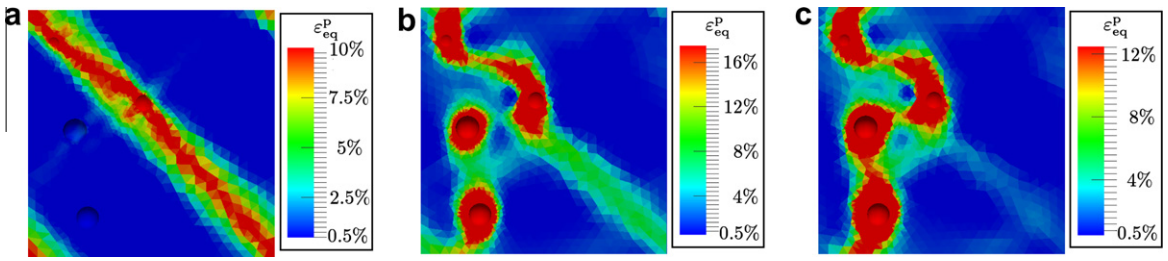

Fig. 15. Distribution of the equivalent plastic strain at the end of the simulation for three load cases with $\alpha = 1$ and $\beta = 0$ (a), 0.25 (b) and 0.50 (c) for a porosity of 1%.

their diameter (Fig. 16). At a porosity of 30%, the diameter of a single pore in an aggregate containing 50 voids is 0.2254 of the edge length of the unit cell. From the analysis of the k-nearest neighbor distance we have found that within this distance 20 or more pores can be found for all of the considered realizations. Accordingly, a large amount of pore–pore interactions occur. For the smallest two porosities, at most one neighboring pore is found within a distance of $2R$. The amount of interaction is, thus, significantly reduced. This is already suggested by the two-point correlation function (Fig. 7).

4. Interpretation and discussion

4.1. Comparison with analytical models

The computational results shown in Fig. 10 have been compared to some of the many existing analytical approaches. Besides the classical Gurson model (Gurson, 1977), the Gurson Hashin–Shtrikman upper bound (Leblond et al., 1994; Garajeu and Suquet, 1997), the Garajeu–Suquet upper bound (Garajeu and Suquet, 1997), the approach of Monchiet et al. (2007) and the approximation proposed by Tvergaard (1981) were chosen. The latter is a phenomenological extension of the original

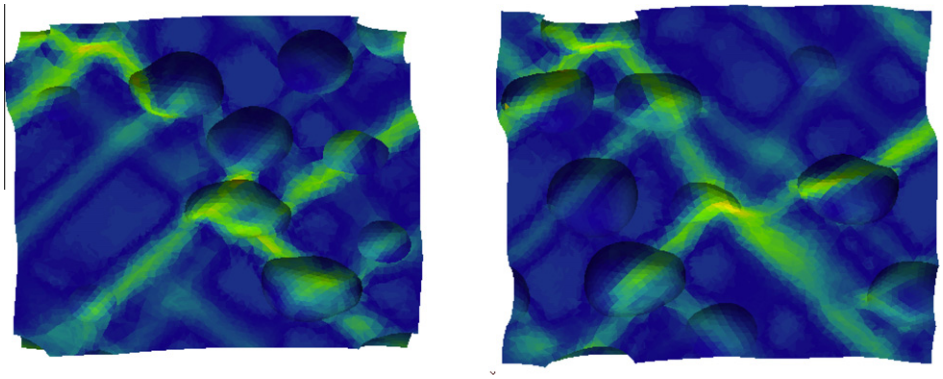

Fig. 16. Distribution of the accumulated plastic strain in a high porosity material (30%); note the small deflections of the localization bands from 45° due to close neighboring pores (load case: $\alpha = 1$, $\beta = 0$); two slices of the entire volume are shown; the deformation is scaled by a factor of 2.

Gurson model by introduction of three coefficients q_1, q_2, $q_3 > 0$. The model is commonly referred to as Gurson–Tvergaard–Needleman (GTN) model. The relation between the macroscopic von Mises equivalent stress and the hydrostatic stress is given by

$$\frac{\Sigma_{\mathrm{eq}}}{\sigma_{\mathrm{F}}} = \sqrt{1 + q_3 f^2 - 2 q_1 f \cosh\left(q_2 \frac{3\Sigma_{\mathrm{m}}}{2\sigma_{\mathrm{F}}}\right)}. \tag{10}$$

Notably, the Gurson model is recovered by setting $q_1 = q_2 = q_3 = 1$. Different values for the coefficients are postulated in the literature (Besson, 2004) with $q_1 = 1.25$–2, $q_2 \approx 1$ and $q_3 = q_1^2$. As stated by various authors in past works related to the topic (see, e.g. Faleskog et al., 1998; Kim et al., 2004) these parameters may depend on different aspects such as the elastic and inelastic material parameters or the pore volume fraction. When trying to adjust the coefficients q_1, q_2, q_3 to the computed data it was immediately found that no set of parameters was able to predict all of the calculated asymptotic stress responses, see for instance Fig. 17 where the high pore volume fractions differ significantly from the model predictions. Additionally, $q_2 = 1$ was found not to reproduce the actual curves with a sufficient accuracy. In particular, the transition from the rather edgy shape for $f = 0.1\%$ to the smooth curve for high porosities ($\geqslant 10\%$) is not possible. For the smaller porosity it was found

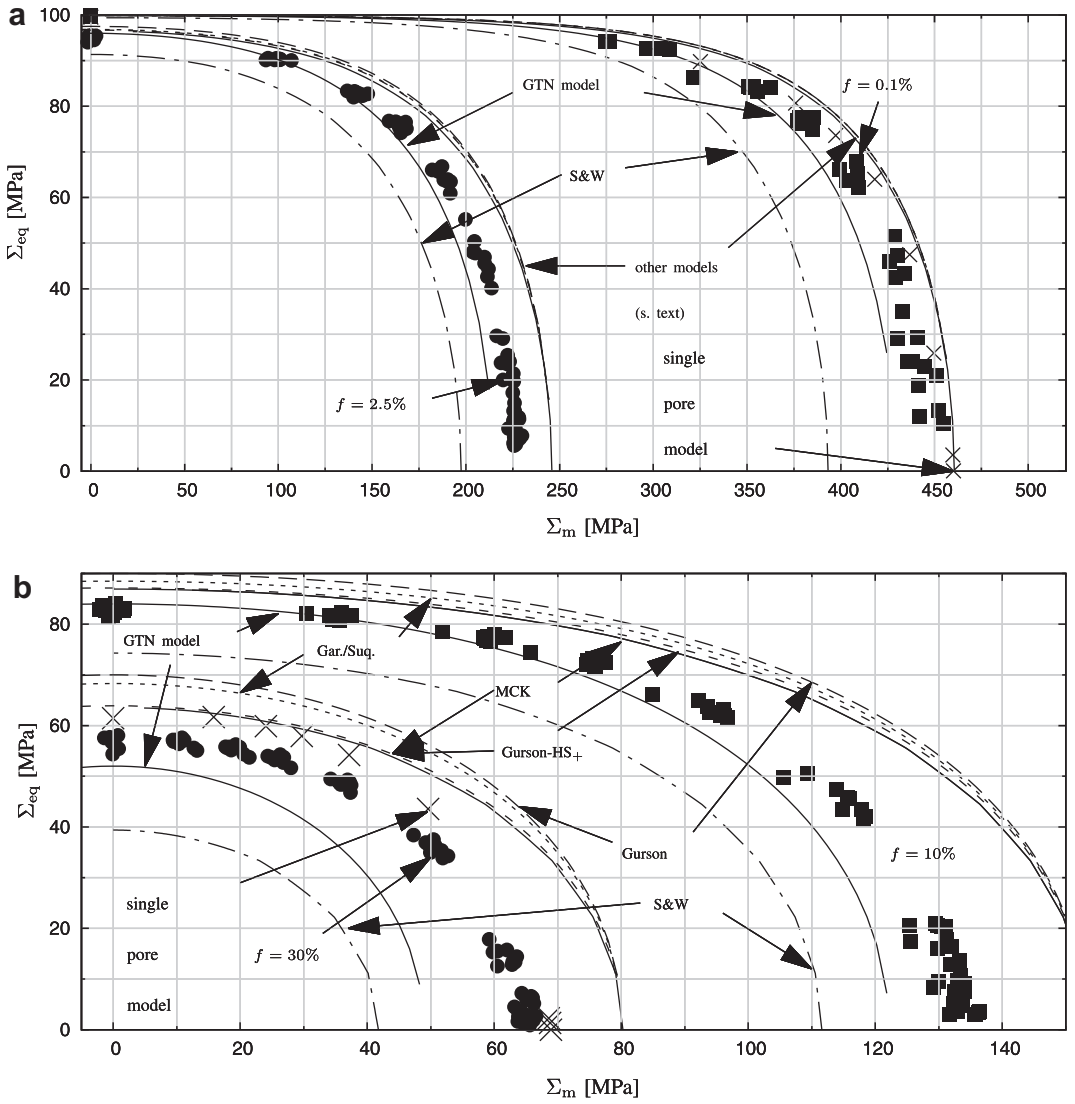

Fig. 17. Comparison of the GTN ($q_1 = 1.5, q_2 = 1, q_3 = q_1^2$), the Gurson-HS estimate (Leblond et al., 1994; Garajeu and Suquet, 1997), the Garajeu–Suquet upper bound (Garajeu and Suquet, 1997), the model by Monchiet et al. (2007) (MCK) and the classical Gurson model with the computational results for $f = 0.1\%$, 2.5% (a) and 10%, 30% (b); the lower bound of Sun and Wang (1995) ($b_4 = 0$; S& W) is also shown.

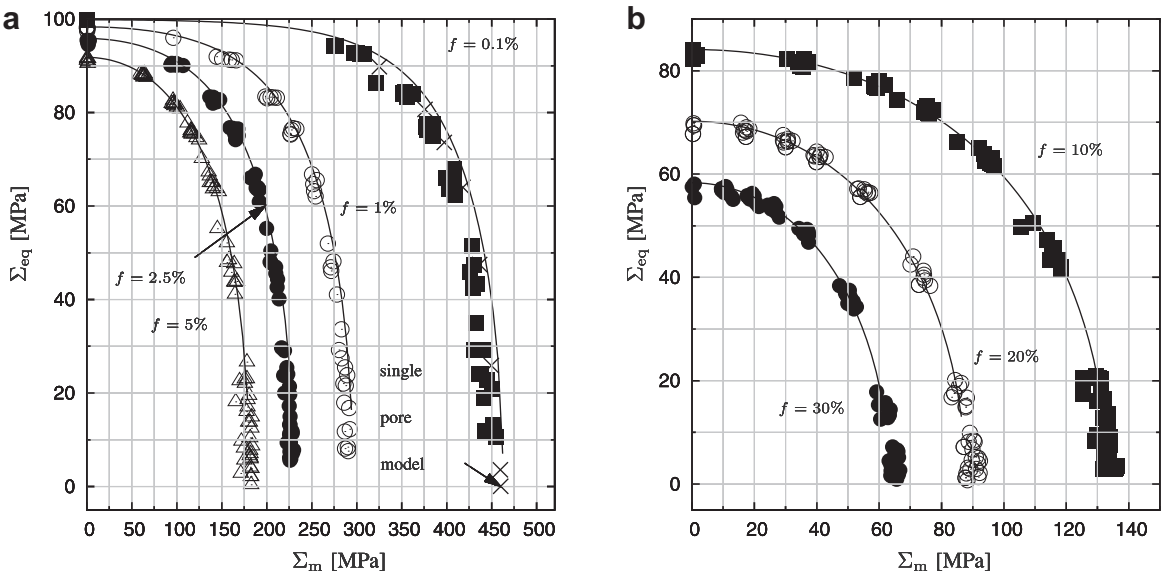

Fig. 18. Adjusted GTN model and computational results.

that all of the analytical models show almost identical behavior (see Fig. 17, top), except for the Gurson model which overestimates the stresses and the GTN model which is a little closer to the computed values.

The consideration of high porosities (10–30%, Fig. 17, bottom) reveals some differences between the different approaches. In summary, the stresses are overpredicted by all models, except the GTN model. The latter does underestimate the stress response for the coefficients determined at the low volume fractions. Note that all computed points satisfy the lower bound of Sun and Wang (1995), where we have chosen $b_4 = 0$. The latter was chosen since for $b_4 > 0$ the predicted stress is even lower. For low pore volume fractions the bound appears to provide some useful estimates. For higher porosities the prediction of the stresses is much too soft in comparison with the computational results and the other analytical models.

4.2. Identification of a modified GTN model

In order to overcome the deficiency of the tested models an adjusted GTN model is proposed based on the presented computational results. Evidently the coefficients q_1, q_2, q_3 are not constant for all volume fractions. This observations complies to

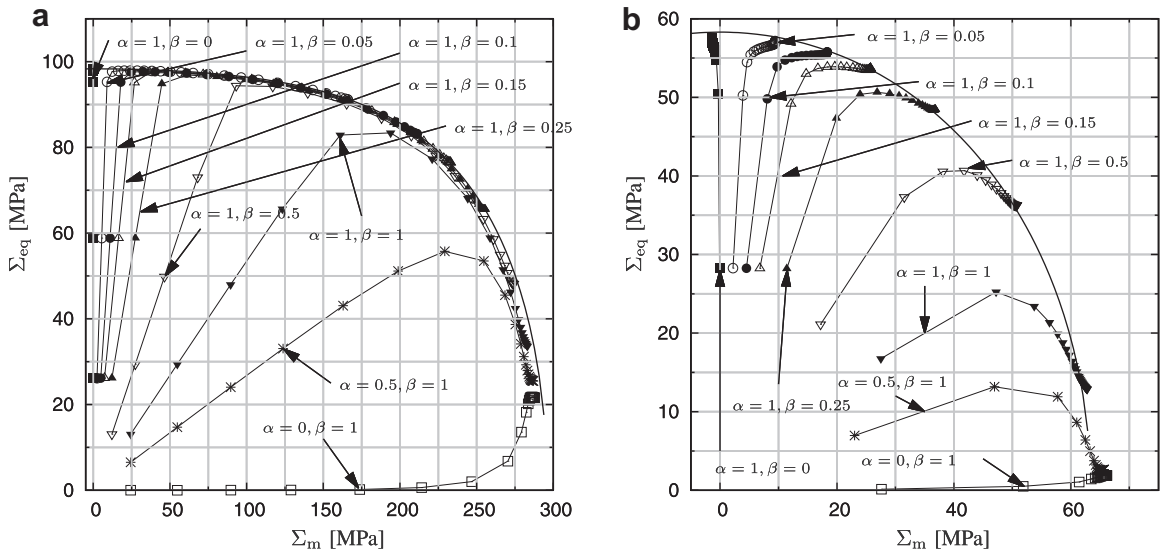

Fig. 19. Time history of the nine investigated load cases for $f = 1\%$ (a) and $f = 30\%$ (b).

the observations of Faleskog et al. (1998) and others which have stated a certain dependency, but who have not provided explicit relations. We found that the simple relations

$$q_1(f) = \theta_0 - \theta_1 f, \quad q_2(f) = \theta_2, \quad q_3(f) = (q_1(f))^2 \tag{11}$$

are sufficient to reproduce the results for the higher volume fractions while the results for the low porosities are still approximated to an excellent extent (Fig. 18). The three scalar coefficients identified based on the computational study are $\theta_0 = 1.69$, $\theta_1 = 1$, $\theta_2 = 0.92$. These parameters have been identified based on a linear regression analysis. The value $\theta_1 = 1$ is remarkable. In the present study the elastic and inelastic material properties were considered constant with the values given in Section 2. For different elastic moduli or a different yield stress the above values should be verified and, if required, re-evaluated from a regression analysis. It should however be taken into account that moderate variations in the ratio σ_F/E have been tested and only minor variations were found. A detailed study of such dependencies is certainly of interest and could give rise to future investigations.

In order to find out the significance of the obtained asymptotic stress response with respect to the loading history, the time history of simulations at 1 and 30% pore volume fraction is shown in Fig. 19 together with the adjusted GTN model. It is found that the simulations do not describe a straight line in the particular choice of stress space but a rather complex non-proportional path. Interestingly, all of the calculated trajectories lie close to the adjusted GTN model, i.e. their position varies almost only tangential to the curve. These results suggest that the proposed model can describe the inelastic response of the structure at all stages of plastic loading and not only in the limit case of an asymptotic response.

5. Conclusions

The macroscopic material behavior of porous materials with perfectly plastic von Mises type plasticity is assessed on a computational basis. The random periodic microstructures consisting of spherical non-intersecting voids described in detail in Section 2 are used in finite element simulations and the deviatoric and hydrostatic limit stresses are captured for all computations (see Section 3). Based on the statistical results presented in Section 2 and results obtained for different types of boundary conditions and numbers of pores in Section 3 the computational results can be considered representative under the stated constitutive assumptions. This result can be considered as a step towards the determination of the size of the representative volume element in this particular physically nonlinear context. In particular, the size of the representative volume element should be determined such that both, suitable statistical descriptors of the unit cell and the macroscopic material response show deviations that are considered acceptable.

For the class of porous materials under consideration it is found that the analytical predictions found in the exhaustive literature on the topic are all rather close to the numerical prediction for small pore volume fractions. The computational study also shows that a single pore model is well suited to approximate the response of a random unit cell containing twenty pores. Notably the analytical models are rather close to the numerical results for pore fractions up to 2.5%. For higher pore fractions significant deviations between the various models are found. Moreover, none of the examined models was able to capture the response at 10–30% volume fraction. Therefore, a modification of the computationally attractive GTN model is proposed. This extension is appealing due to a single additional parameter and its ability to fit all calculated points to an excellent extent. Due to the simplicity of the model adjustment, existing implementations of the GTN model can easily be adapted, e.g. the *Impl-Ex-Method* used in Sánchez et al. (2008).

Future research can be dedicated to the consideration of more general loading conditions and of the role played by the third invariant of the stress tensor. Such studies could, e.g., consider explicit variation of the Lode angle which is near constant in our investigations (see Section 3.3). The proposed computational approach could then be extended to tackle anisotropic properties of the matrix, for instance of pores found in single crystals (see Yerra et al., 2010) and pore size effects in the case of strain gradient plasticity matrix behavior (see Li and Steinmann, 2006). An additional point of interest are geometrically nonlinear investigations which can account not only for the asymptotic stress response but which may also provide information with respect to the evolution of the void volume fraction and the void morphology.

Acknowledgement.

This work was supported by the Karlsruhe House of Young Scientists (KHYS) of the Karlsruhe Institute of Technology.

References

Benzerga, A., Leblond, J.B., 2010. Ductile fracture by void growth to coalescence. Advances in Applied Mechanics 44, 169–305.
Besson, J., 2004. Local Approach to Fracture. Ecole des Mines de Paris–Les Presses.
Besson, J., 2009. Damage of ductile materials deforming under multiple plastic or viscoplastic mechanisms. International Journal of Plasticity 25, 2204–2221.
Besson, J., 2010. Continuum models of ductile fracture: a review. International Journal of Damage Mechanics 19, 3–52.
Bilger, N., Auslender, F., Bornert, M., Michel, J.-C., Moulinec, H., Suquet, P., Zaoui, A., 2005. Effect of a nonuniform distribution of voids on the plastic response of voided materials: a computational and statistical analysis. International Journal of Solids and Structures 42 (2), 517–538.
Bilger, N., Auslender, F., Bornert, M., Moulinec, H., Zaoui, A., 2007. Bounds and estimates for the effective yield surface of porous media with a uniform or a nonuniform distribution of voids. European Journal of Mechanics – A/Solids 26 (5), 810–836.
Böhlke, T., 2004. The Voigt bound of the stress potential of isotropic viscoplastic fcc polycrystals. Archive of Mechanics 56 (6), 423–443.

Cailletaud, G., Forest, S., Jeulin, D., Feyel, F., Galliet, I., Mounoury, V., Quilici, S., 2003. Some elements of microstructural mechanics. Computational Materials Science 27, 351–374.
Danas, K., Idiart, M., Castañeda, P.P., 2008. A homogenization-based constitutive model for isotropic viscoplastic porous media. International Journal of Solids and Structures 45 (11–12), 3392–3409.
Danas, K., Ponte-Castañeda, P., 2009a. A finite-strain model for anisotropic viscoplastic porous media: I – theory. European Journal of Mechanics – A/Solids 28 (3), 387–401.
Danas, K., Ponte-Castañeda, P., 2009b. A finite-strain model for anisotropic viscoplastic porous media: Ii – applications. European Journal of Mechanics – A/Solids 28 (3), 402–416.
Faleskog, J., Gao, X., Shih, C., 1998. Cell model for nonlinear fracture analysis – I. micromechanics calibration. International Journal of Fracture 89, 355–373, 10.1023/A:1007421420901.
Fritzen, F., Böhlke, T., Schnack, E., 2009. Periodic three-dimensional mesh generation for crystalline aggregates based on voronoi tessellations. Computational Mechanics 43 (5), 701.
Gao, X., Zhang, T., Hayden, M., Roe, C., 2009. Effects of the stress state on plasticity and ductile failure of an aluminum 5083 alloy. International Journal of Plasticity 25 (12), 2366–2382.
Gao, X., Zhang, T., Zhou, J., Graham, S.M., Hayden, M., Roe, C., 2011. On stress-state dependent plasticity modeling: Significance of the hydrostatic stress, the third invariant of stress deviator and the non-associated flow rule. International Journal of Plasticity 27 (2), 217–231.
Garajeu, M., Suquet, P., 1997. Effective properties of porous ideally plastic or viscoplastic materials containing rigid particles. Journal of the Mechanics and Physics of Solids 45 (6), 873–902.
Ghosh, S., Bai, J., Paquet, D., 2009. Homogenization-based continuum plasticity-damage model for ductile failure of materials containing heterogeneities. Journal of the Mechanics and Physics of Solids 57, 1017–1044.
Gibson, L., Ashby, M., 1997. Cellular solids: structure and properties, second ed. Edition. Cambridge solid state science series. Cambridge Univ. Pr., Cambridge, includes bibliographical references and index – Previous ed.: Oxford: Pergamon, 1988.
Gitman, I., Askes, H., Sluys, L., 2007. Representative volume: existence and size determination. Engineering Fracture Mechanics 74, 2518–2534.
Gologanu, M., Leblond, J., Devaux, J., 1997. Continuum micromechanics. CISM Courses and Lectures Ch. Recent Extensions of Gurson's Model for Porous Ductile Metals, vol. 377. Springer Verlag, pp. 61–130.
Guo, T., Faleskog, J., Shih, C., 2008. Continiuum modeling of a porous solid with pressure-sensitive dilatant matrix. Journal of the Mechanics and Physics of Solids 56, 2188–2212.
Gurson, A., 1977. Continuum theory of ductile rupture by void nucleation and growth. Part I – yield criteria and flow rules for porous ductile media. Journal for Engineering Materials and Technology 99, 2–15.
Gusev, A.A., 1997. Representative volume element size for elastic composites: a numerical study. Journal of the Mechanics and Physics of Solids 45, 1449–1459.
Hazanov, S., Huet, C., 1994. Order relationships for boundary conditions effect in heterogeneous bodies smaller than the representative volume. Journal of the Mechanics and Physics of Solids 42, 1995–2011.
Hsu, C., Lee, B., Mear, M., 2009. Constitutive models for power-law viscous solids containing spherical voids. International Journal of Plasticity 25 (1), 134–160.
Jessell, M.W., Bons, P.D., Griera, A., Evans, L.A., Wilson, C.J.L., 2009. A tale of two viscosities. Journal of Structural Geology 31, 719–736.
Kanit, T., Forest, S., Galliet, I., Mounoury, V., Jeulin, D., 2003. Determination of the size of the representative volume element for random composites: statistical and numerical approach. International Journal of Solids and Structures 40, 3647–3679.
Kanit, T., N'Guyen, F., Forest, S., Jeulin, D., Reed, M., Singleton, S., 2006. Apparent and effective physical properties of heterogeneous materials: representativity of samples of two materials from food industry. Computer Methods in Applied Mechanics and Engineering 195 (33-36), 3960–3982.
Kim, J., Gao, X., Srivatsan, T.S., 2004. Modeling of void growth in ductile solids: effects of stress triaxiality and initial porosity. Engineering Fracture Mechanics 71 (3), 379–400.
Leblond, J.B., Perrin, G., Suquet, P., 1994. Exact results and approximate models for porous viscoplastic solids. International Journal of Plasticity 10 (3), 213–235.
Li, Z.H., Steinmann, P., 2006. RVE-based studies on the coupled effects of void size and void shape on yield behavior and void growth at micron scales. International Journal of Plasticity 22, 1195–1216.
Madi, K., Forest, S., Cordier, P., Boussuge, M., 2005. Numerical study of creep in two-phase aggregates with a large rheology contrast: implications for the lower mantle. Earth and Planetary Science Letters 237, 223–238.
Michel, J., Moulinec, H., Suquet, P., 2001. A computational scheme for linear and non-linear composites with arbitrary phase contrast. International Journal for Numerical Methods in Engineering 52 (1–2), 139–160.
Michel, J.C., Suquet, P., 1992. The constitutive law of nonlinear viscous and porous materials. Journal of the Mechanics and Physics of Solids 40 (4), 783–812.
Monchiet, V., Cazacu, O., Charkaluk, E., Kondo, D., 2008. Macroscopic yield criteria for plastic anisotropic materials containing spheroidal voids. International Journal of Plasticity 24 (7), 1158–1189.
Monchiet, V., Charkaluk, E., Kondo, D., 2007. An improvement of gurson-type models of porous materials by using Eshelby-like trial velocity fields. Comptes Rendus MTcanique 335 (1), 32–41.
Monchiet, V., Charkaluk, E., Kondo, D., 2011. A micromechanics-based modification of the Gurson criterion by using Eshelby-like velocity fields. European Journal of Mechanics – A/Solids 30 (6), 940–949.
Moulinec, H., Suquet, P., 1998. A numerical method for computing the overall response of nonlinear composites with complex microstructure. Computer Methods in Applied Mechanics and Engineering 157, 69–94.
Needleman, A., Tvergaard, V., 1984. An analysis of ductile rupture in notched bars. Journal of the Mechanics and Physics of Solids 32 (6), 461–490.
Needleman, A., Tvergaard, V., 1987. An analysis of ductile rupture modes at a crack tip. Journal of the Mechanics and Physics of Solids 35 (2), 151–183.
Nemat-Nasser, S., Hori, M., 1999. Micromechanics: Overall Properties of Heterogeneous Materials. Elsevier.
Pardoen, T., Pineau, A., 2007. Comprehensive Structural Integrity. In: Milne, I., Ritchie, R.O., Karihaloo, B. (Eds.), Ch. Failure mechanisms of metals, vol. 2. Elsevier, pp. 684–797 (Chapter 6).
Perrin, G., 1992. Contribution à l'etude théorique et numérique de la rupture ductile des métaux. Ph.D., Ecole Polytechnique Palaiseau, France.
Ponte-Castañeda, P., 1991. The effective mechanical properties of nonlinear isotropic composites. Journal of the Mechanics and Physics of Solids 39 (1), 45–71.
Ranganathan, S., Ostoja-Starzewski, M., 2008. Scaling function, anisotropy and the size of rve in elastic random polycrystals. Journal of the Mechanics and Physics of Solids 56 (9), 2773–2791.
Ren, Z.-Y., Zheng, Q.-S., 2002. A quantitative study of minimum sizes of representative volume elements of cubic polycrystals-numerical experiments. Journal of the Mechanics and Physics of Solids 50, 881–893.
Sab, K., Nedjar, B., 2005. Periodization of random media and representative volume element size for linear composites. ***C.R. Mécanique 333, 187–195.
Schöberl, J., 1997. Netgen an advancing front 2d/3d-mesh generator based on abstract rules. Computing and Visualization in Science 1 (1), 41–52.
Seifert, T., Schmidt, I., 2009. Plastic yielding in cyclically loaded porous materials. International Journal of Plasticity 25 (12), 2435–2453.
Sánchez, P., Huespe, A., Oliver, J., 2008. On some topics for the numerical simulation of ductile fracture. International Journal of Plasticity 24 (6), 1008–1038.
Sun, Y., Wang, d., 1995. Analysis of shear localization in porous materials based on a lower bound approach. International Journal of Fracture 71, 71–83.
Suquet, P., 1992. On bounds for the overall potential of power law materials containing voids with an arbitrary shape. Mechanics Research Communications 19 (1), 51–58.
Torquato, S., 2002. Random Heterogeneous Materials: Microstructure and Macroscopic Properties. Springer, New York [u.a.].

Trillat, M., Pastor, J., 2005. Limit analysis and Gurson's model. European Journal of Mechanics A/solids 24, 800–819.
Tvergaard, V., 1981. Influence of voids on shear band instabilities under plane strain conditions. International Journal of Fracture 17 (4), 389–407.
Yerra, S., Tekoglu, C., Scheyvaerts, F., Delannay, L., Van Houtte, P., Pardoen, t., 2010. Void growth and coalescence in single crystals. International Journal of Solids Structures 47, 1016–1029.